

One Size Does Not Fit All: A Distribution-Aware Sparsification for More Precise Model Merging

Yingfeng Luo ^{1*}, Dingyang Lin ^{1*}, Junxin Wang ¹, Ziqiang Xu ¹, Kaiyan Chang ¹, Tong Zheng ¹, Bei Li ¹, Anxiang Ma ¹, Tong Xiao ^{1,2†}, Zhengtao Yu ³, Jingbo Zhu ^{1,2}

¹ School of Computer Science and Engineering, Northeastern University, Shenyang, China

² NiuTrans Research, Shenyang, China

³ Kunming University of Science and Technology, Kunming, China

luoyingfeng.neu@outlook.com

{xiaotong, zhujingbo}@mail.neu.edu.cn

Abstract

Model merging has emerged as a compelling data-free paradigm for multi-task learning, enabling the fusion of multiple fine-tuned models into a single, powerful entity. A key technique in merging methods is sparsification, which prunes redundant parameters from task vectors to mitigate interference. However, prevailing approaches employ a “one-size-fits-all” strategy, applying a uniform sparsity ratio that overlooks the inherent structural and statistical heterogeneity of model parameters. This often leads to a suboptimal trade-off, where critical parameters are inadvertently pruned while less useful ones are retained. To address this limitation, we introduce **TADrop** (Tensor-wise Adaptive Drop), an adaptive sparsification strategy that respects this heterogeneity. Instead of a global ratio, TADrop assigns a tailored sparsity level to each parameter tensor based on its distributional properties. The core intuition is that tensors with denser, more redundant distributions can be pruned aggressively, while sparser, more critical ones are preserved. As a simple and plug-and-play module, we validate TADrop by integrating it with foundational, classic, and SOTA merging methods. Extensive experiments across diverse tasks (vision, language, and multimodal) and models (ViT, BEiT) demonstrate that TADrop consistently and significantly boosts their performance. For instance, when enhancing a leading merging method, it achieves an average performance gain of 2.0% across 8 ViT-B/32 tasks. TADrop provides a more effective way to mitigate parameter interference by tailoring sparsification to the model’s structure, offering a new baseline for high-performance model merging.

Introduction

In the era of rapid advancements in AI, pre-trained models (PTMs) have become the cornerstone of modern machine learning, where the standard practice of fine-tuning them on specific downstream tasks has driven breakthroughs in natural language processing (Devlin et al. 2019; Radford and Narasimhan 2018; Xiao and Zhu 2025; Luo et al. 2025; Chang et al. 2024), computer vision (Kolesnikov et al. 2019), and multimodal tasks (Radford et al. 2021). However,

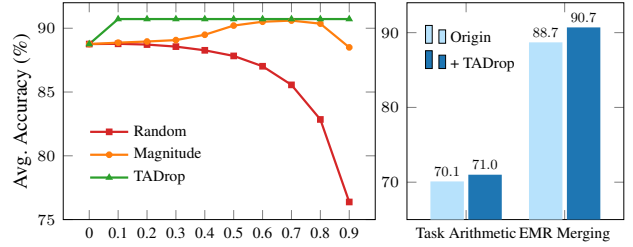


Figure 1: Performance evaluation of TADrop on model merging across 8 ViT-B/32 models. Left: Impact of different sparsity strategies (Sparsity Rate) on merged model accuracy. Right: performance gains across merging methods.

as the number of tasks grows exponentially—encompassing diverse domains, modalities, and data scales—a critical challenge emerges: the high costs of storing, computing, and deploying multiple task-specific models. Moreover, independently fine-tuning these models prevents them from leveraging knowledge across related tasks for improved performance (Sanh et al. 2022; Raffel et al. 2020).

A well-established strategy to address these limitations is Multi-Task Learning (MTL) (Zhang and Yang 2022). By jointly training a single, shared model on data from multiple tasks, it directly tackles the issues of knowledge silos and model proliferation. However, the practical application of MTL is constrained by two major hurdles in the modern foundation model era (Yu et al. 2020; Zhang and Yang 2022). First, data availability has become a critical bottleneck. A significant trend in the current ecosystem is that practitioners are more inclined to release their fine-tuned models, while the underlying training data remains proprietary due to privacy, security, or commercial concerns. This reality of “open models, closed data” makes the traditional MTL paradigm impractical in many real-world scenarios. Second, even when the data is available, the computational cost of jointly fine-tuning large-scale foundation models across numerous datasets is often prohibitive.

Model merging (Yang et al. 2024a) has recently emerged as a compelling solution, fusing multiple models in param-

*These authors contributed equally.

†Corresponding author.

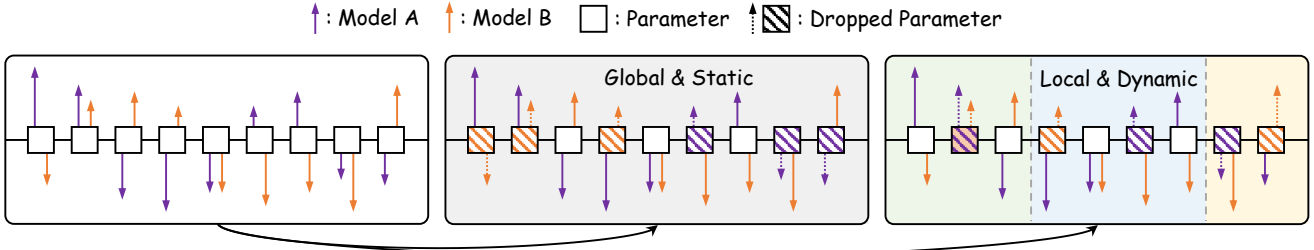


Figure 2: Conceptual illustration of TADrop. The figure contrasts conventional global sparsification with our adaptive TADrop. While global methods (center) apply a uniform drop rate to the initial task vectors (left), our TADrop (right) operates at the tensor-level, applying a tailored drop rate to each tensor based on its unique characteristics (visualized by colored regions).

eter space without requiring access to original data or additional training. Early merging methods, such as weight averaging (Wortsman et al. 2022), often lead to a significant degradation in performance due to parameter interference. A milestone advancement was the introduction of the *Task Vector* (Ilharco et al. 2023), which merges only the task vectors—defined as the differences between the fine-tuned and pre-trained model parameters—rather than the full models. This approach decouples the pretrained model’s knowledge, effectively mitigates interference, and has become a foundational approach. Later, the discovery that these vectors exhibit substantial redundancy (Yu et al. 2024) established sparsification as a foundational pre-processing step to mitigate parameter interference by dropping less informative parameters. This has spurred a variety of techniques aimed at identifying and combining critical parameters (Yadav et al. 2023; Wang et al. 2024; Yang et al. 2024b; Du et al. 2024; Zhang et al. 2025; He et al. 2025; Yang et al. 2025b,a).

However, while a variety of sparsification techniques exist, the dominant and most widely adopted approaches still rely on a “one-size-fits-all” global threshold, treating entire networks as high-dimensional vectors. This flattened view overlooks the model’s inherent structural hierarchy, where parameters are not a flat collection but are nested within functional modules (like attention and feed-forward), which in turn are stacked into layers. Ignoring this structure is a notable oversight, as it gives rise to parameter heterogeneity: as shown in Figure 3, parameters residing in different modules and layers exhibit vastly different statistical distributions and sensitivities to pruning. Consequently, applying a single, global sparsification threshold is inherently suboptimal, forcing a poor trade-off where critical parameters are aggressively pruned while redundant ones are retained.

To address the challenge of parameter heterogeneity, we propose **TADrop** (Tensor-wise Adaptive **D**rop), a fine-grained and dynamically adaptive sparsification strategy. As shown in Figure 2, instead of a fixed global drop ratio, TADrop operates at the tensor level, assigning each tensor a tailored drop rate dynamically estimated from its distributional properties. The core principle is intuitive: tensors with denser distributions are likely more redundant and can be pruned aggressively, while those with sparser distributions may contain critical information and are thus pruned more conservatively. By tailoring sparsity to each

tensor’s characteristics, TADrop resolves the suboptimal trade-offs of global methods, simultaneously protecting critical sparse parameters while surgically removing redundancy from dense, less-informative ones. As a simple, plug-and-play module, TADrop is fully compatible with existing model merging frameworks. We validate the effectiveness and generality of TADrop through extensive experiments spanning a spectrum of merging methods as well as diverse task modalities, including vision, language, and multimodal applications. As shown in Figure 1, TADrop yields consistent and significant performance gains across the tested baselines, boosting a leading SOTA method by a substantial 2.0% in average accuracy across 8 ViT-B/32 tasks.

In summary, our main contributions are threefold:

- We identify and analyze the limitations of “one-size-fits-all” sparsification strategies, highlighting the problem of parameter heterogeneity in model merging.
- We propose TADrop, a simple, plug-and-play, and fine-grained sparsification method that adaptively tailors drop ratios at the tensor level to resolve the limitations of global approaches.
- We demonstrate that our method delivers substantial performance gains over baselines across a wide range of tasks and models, confirming its effectiveness.

Related Work

Multi-Task Learning (MTL) has been a long-standing pursuit in machine learning, aiming to create a single model that can handle multiple tasks to improve efficiency and generalization (Caruana 1997; Zhang and Yang 2022). The conventional approach, joint training, trains a shared model on data from all tasks simultaneously. However, this paradigm faces two critical hurdles in the era of foundation models. First, it requires simultaneous access to all training datasets, an assumption that is often untenable due to data privacy. Second, the computational cost of jointly fine-tuning large-scale models is often prohibitive.

In this context, model merging (Yang et al. 2024a) has recently emerged as a compelling, data-free alternative for achieving multi-task capabilities. This paradigm directly combines multiple fine-tuned, task-specific models into a single multi-task model through arithmetic operations in the

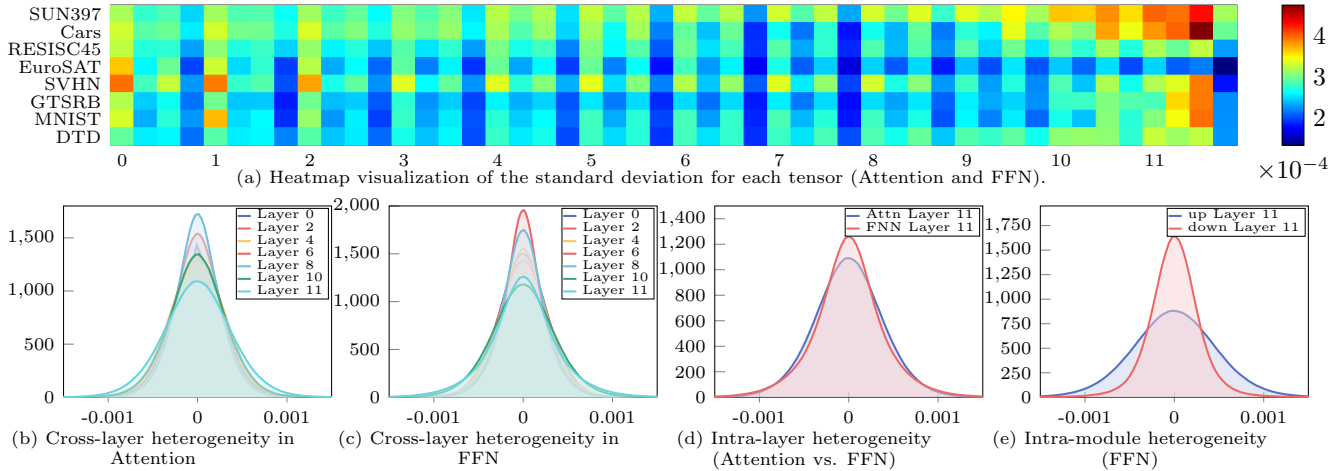


Figure 3: Visualization of parameter heterogeneity in task vectors at multiple levels. Together, these results highlight the pervasive heterogeneity in parameter distributions across tasks, layers, modules, and subcomponents.

parameter space, thus circumventing the need for raw data and costly retraining. Early attempts, such as naively averaging all model weights (Wortsman et al. 2022), largely failed due to severe parameter interference, where conflicting task-specific knowledge was destroyed during the merging process. The introduction of the *Task Vector* (Ilharco et al. 2023) marked a significant breakthrough. A task vector—the difference between a fine-tuned model and its pre-trained base—isolates task-specific modifications, thereby preserving the shared knowledge of the foundation model.

Building upon the task vector paradigm, subsequent research has focused on how to further “purify” and “allocate” these vectors. A dominant line of work centers on resolving inter-task conflicts through pruning and balancing strategies. Ties-Merging (Yadav et al. 2023) prunes parameters based on magnitude and resolves sign disagreements. DELLA-Merging (Deep, Bhardwaj, and Poria 2024) proposes magnitude-based sampling to drop conflicting deltas while preserving salient task-specific signals. Similarly, CABS (Yang et al. 2025b) adopts a two-stage process to reduce task vector overlap and ensure balanced sparsity across layers. Furthermore, Localize-and-Stitch (He et al. 2025) focuses on identifying critical sparse structures to retain during merging, though it requires some task-specific data. SVD-based methods like ImPart (Yang et al. 2025a) and AdaRank (Lee et al. 2025) prune singular directions based on their contribution to task-specific knowledge or interference reduction. Another research direction explores learning adaptive merging coefficients for each task vector (Yang et al. 2024b), or retaining a small set of dedicated, task-specific parameters (Wang et al. 2024; Huang et al. 2024).

While these advanced techniques have demonstrated considerable success, we argue that their approach to handling intra-task redundancy remains underdeveloped. A key limitation of these approaches is their tendency to treat the parameters within each task vector as a homogeneous set, often applying “one-size-fits-all” sparsification. This overlooks the critical issue of parameter heterogeneity—the fact that

different parameter groups within a single task vector have different statistical properties and importance. Our work is built upon the insight that a more granular and adaptive approach to intra-task redundancy is required. Therefore, our proposed method, **TADrop**, shifts focus from inter-task conflict resolution to meticulously managing intra-task redundancy. Unlike existing sparsification strategies that prune uniformly across or within layers, TADrop adopts an intra-vector perspective by assessing the statistical distribution of each tensor within a task vector. This enables TADrop to assign adaptive sparsification rates to each tensor based on its inherent redundancy, thus avoiding the pitfalls of one-size-fits-all pruning. Notably, TADrop is data-free and can serve as a complementary pre-processing step to enhance existing merging methods.

Methodology

Preliminaries

Our research is set within the current mainstream “pretraining-finetuning” paradigm. We begin with a publicly available pre-trained model, whose parameters are denoted as a set of n tensors, $\theta_{pre} = \{\theta_{pre}^1, \theta_{pre}^2, \dots, \theta_{pre}^n\}$. This pre-trained model is independently fine-tuned on K distinct downstream tasks, yielding K task-specific models, each with its own parameter set $\theta_k = \{\theta_k^1, \theta_k^2, \dots, \theta_k^n\}$. The goal of model merging is to devise a fusion function $\mathcal{F}(\cdot)$ that can integrate the these K models’s weights $\{\theta_k\}_{k=1}^K$ into a single multi-task model θ_{MTL} that performs well across all K tasks, without access to the original training data.

A naive approach like weight averaging (Wortsman et al. 2022), i.e., $\theta_{MTL} = 1/K \sum_{k=1}^K \theta_k$, is straightforward, while it often suffers from severe performance degradation due to parameter interference across tasks. To better address this challenge, modern model merging methods (Jin et al. 2023; Yadav et al. 2023; Yang et al. 2024b; Matena and Raffel 2022; Huang et al. 2024) predominantly build upon the *Task Vector* (Ilharco et al. 2023) paradigm. The task vector

τ_k for a task k is defined as the difference between the fine-tuned and pre-trained parameters:

$$\tau_k = \theta_k - \theta_{pre} \quad (1)$$

Intuitively, τ_k captures the “modification” or “incremental knowledge” applied to the pretrained model to adapt it for task k . Task vector-based merging typically combines these vectors linearly and adds the result back to the original pre-trained weights to construct the multi-task model. The general form of this operation is:

$$\theta_{MTL} = \theta_{pre} + \sum_{k=1}^K \lambda_k \tau_k \quad (2)$$

where λ_k is the merging coefficient for task k . To further alleviate parameter interference, most advanced methods (Jin et al. 2023; Yadav et al. 2023; Matena and Raffel 2022; Huang et al. 2024) introduce a series of pre-processing operations on each task vector before aggregation. We can represent these operations collectively as a transformation operator $\Phi(\cdot)$, yielding a more generalized merging framework:

$$\theta_{MTL} = \theta_{pre} + \sum_{k=1}^K \lambda_k \Phi(\tau_k) \quad (3)$$

While some recent methods introduce additional components or masks (Huang et al. 2024; Wang et al. 2024; Du et al. 2024; Lu et al. 2024), this formulation effectively captures the dominant paradigm of modifying and combining task vectors. Within this framework, one of the most crucial steps in the operator $\Phi(\cdot)$ is sparsification. Our work focuses on revisiting and redesigning this critical step.

Motivation

The prevailing “one-size-fits-all” sparsification strategies are built upon an implicit, yet critical, assumption: that task vectors are a homogeneous set of parameters. We challenge this premise through an empirical analysis of ViT-B/16 models (Dosovitskiy et al. 2021), demonstrating that parameter heterogeneity is, in fact, an intrinsic property of task vectors across multiple levels of granularity.

Our multi-faceted investigation, visualized in Figure 3, reveals a pervasive pattern of non-uniformity: first, at the macro inter-task level, different tasks exhibit unique statistical fingerprints. The heatmap in Figure 3a shows that the magnitude and pattern of parameter modifications vary drastically across tasks. For instance, the task vector for SUN397 shows high variance in the final layers, whereas the vector for EuroSAT has a consistently low variance throughout. Second, zooming into the intra-model level (using SUN397 as an example), we observe significant heterogeneity across the model’s architecture. Parameter distributions not only differ across layers for both Attention and FFN modules (Figure 3b, Figure 3c) but also diverge between different module types within the same layer (Figure 3d). Finally, at the most granular intra-module level, Figure 3e reveals clear statistical discrepancies even between the tightly coupled linear layers (up- and down-projection) within a single FFN block.

Drawing upon this multi-level evidence, from the macro task-level to the micro component-level, we argue that treating these statistically and functionally diverse parameters as a homogeneous set is unreasonable. Consequently, applying a single, global sparsification threshold inevitably forces a suboptimal trade-off between information preservation and redundancy removal. This insight makes it desirable to develop a fine-grained, adaptive strategy that can perceive and leverage this intrinsic heterogeneity, which forms the motivation for our proposed method, TADrop.

TADrop

The core principle of TADrop is to abandon the uniform global sparsity rate and, instead, dynamically compute and assign a sparsity rate that is tailored to each parameter tensor in the task vector based on its own distributional characteristics. To achieve this, we require a metric that is both computationally efficient and effective at quantifying the heterogeneity observed in our motivation section. Our analysis revealed that the parameter distributions, while varied, often resemble normal or heavy-tailed distributions. Motivated by this, we propose a simple yet effective metric: the Quantile Ratio. We hypothesize that the more “heavy-tailed” the absolute value distribution of a tensor’s parameters is—meaning it possesses more high-magnitude values—the more critical task-specific information it contains, and thus the lower its redundancy. For the task tensor $\tau_k = \{\tau_k^1, \tau_k^2, \dots, \tau_k^n\}$, we compute the quantile ratio for each tensor τ_k^i as:

$$d_k^i = \frac{Q_a(|\tau_k^i|)}{Q_b(|\tau_k^i|) + \epsilon} \quad (4)$$

where $|\tau_k^i|$ denotes the absolute value of all elements in the tensor, and $Q_p(\cdot)$ is the function that computes the p -th quantile of a set. The parameters a and b are preset quantiles, satisfying $0 < a < b < 1$, and ϵ is a small constant to prevent division by zero. This ratio d_k^i is highly intuitive: if the absolute value distribution of a tensor is heavy-tailed (i.e., many high-magnitude parameters exist), its upper quantile Q_b will be significantly larger than its lower quantile Q_a , resulting in a small value for d_k^i , and vice versa. Therefore, we directly use d_k^i as the adaptive drop rate for the tensor, setting the fraction d_k^i of parameters with the lowest absolute values to zero for each tensor. This ensures that tensors deemed more critical are sparsified less aggressively, while more redundant tensors are pruned more heavily.

Magnitude-based sparsification alters the overall magnitude (as measured by the L2 norm) of a tensor, which could introduce unintended imbalances during aggregation. To counteract this effect, we introduce a norm-preserving scaling step after sparsification. Let $\hat{\tau}_k^i$ be the tensor after being sparsified with the drop rate d_k^i . We then scale it to obtain the final tensor $\tau_k'^i$:

$$\tau_k'^i = \hat{\tau}_k^i \cdot \frac{\|\tau_k^i\|_2}{\|\hat{\tau}_k^i\|_2 + \epsilon} \quad (5)$$

This step ensures that the L2 norm of each tensor is restored to its original value after the TADrop operation.

| Methods | SUN397 | Cars | RESISC45 | EuroSAT | SVHN | GTSRB | MNIST | DTD | Avg. Acc |
|---------------------|---------------------------|---------------------------|---------------------------|---------------------------|---------------------------|---------------------------|---------------------------|---------------------------|---------------------------|
| Individual | 79.2 / 84.9 | 77.7 / 92.4 | 96.1 / 97.4 | 99.7 / 99.7 | 97.5 / 98.1 | 98.7 / 99.2 | 99.7 / 99.8 | 79.4 / 84.1 | 91.0 / 94.4 |
| Traditional MTL | 73.9 / 80.8 | 74.4 / 90.6 | 93.9 / 96.3 | 98.2 / 96.3 | 95.8 / 97.6 | 98.9 / 99.1 | 99.5 / 99.6 | 77.9 / 84.4 | 88.9 / 93.5 |
| Weight Averaging | 65.3 / 72.1 | 63.4 / 81.6 | 71.4 / 82.6 | 71.7 / 91.9 | 64.2 / 78.2 | 52.8 / 70.7 | 87.5 / 97.1 | 50.1 / 62.8 | 65.8 / 79.6 |
| Fisher Merging | 68.6 / 69.2 | 69.2 / 88.6 | 70.7 / 87.5 | 66.4 / 93.5 | 72.9 / 80.6 | 51.1 / 74.8 | 87.9 / 93.3 | 59.9 / 70.0 | 68.3 / 82.2 |
| RegMean | 65.3 / 73.3 | 63.5 / 81.8 | 75.6 / 86.1 | 78.6 / 97.0 | 78.1 / 88.0 | 67.4 / 84.2 | 93.7 / 98.5 | 52.0 / 60.8 | 71.8 / 83.7 |
| PCB-Merging | 66.7 / 76.8 | 65.5 / 86.2 | 78.5 / 89.4 | 79.3 / 96.5 | 86.4 / 88.3 | 77.1 / 91 | 98.2 / 98.6 | 59.1 / 73.6 | 76.3 / 87.5 |
| Localize-and-Stitch | 67.2 / - | 68.3 / - | 81.8 / - | 89.4 / - | 87.9 / - | 86.6 / - | 94.8 / - | 62.9 / - | 79.9 / - |
| AdaMerging++ | 66.6 / 79.4 | 68.3 / 90.3 | 82.2 / 91.6 | 94.2 / 97.4 | 89.6 / 93.4 | 89.0 / 97.5 | 98.3 / 99.0 | 60.6 / 79.2 | 81.1 / 91.0 |
| ProDistill | 68.9 / 77.7 | 71.2 / 90.0 | 89.9 / 94.4 | 99.4 / 99.5 | 96.1 / 97.7 | 95.3 / 98.3 | 99.5 / 99.6 | 68.0 / 78.2 | 86.0 / 91.9 |
| Task Arithmetic | 63.8 / 74.1 | 62.1 / 82.1 | 72.0 / 86.7 | 77.6 / 93.8 | 74.4 / 87.9 | 65.1 / 86.8 | 94.0 / 98.9 | 52.2 / 65.6 | 70.1 / 84.5 |
| + TADrop | 62.7 / 74.3 | 61.7 / 82.9 | 72.2 / 87.3 | 78.2 / 93.5 | 77.4 / 88.1 | 67.5 / 87.7 | 95.9 / 99.0 | 52.2 / 66.8 | 71.0 / 84.9 |
| Ties-Merging | 64.8 / 76.5 | 62.9 / 85.0 | 74.3 / 89.3 | 78.9 / 95.7 | 83.1 / 90.3 | 71.4 / 83.3 | 97.6 / 99.0 | 56.2 / 68.8 | 73.6 / 86.0 |
| + TADrop | 64.8 / 76.0 | 63.0 / 83.6 | 74.1 / 88.5 | 82.1 / 94.3 | 81.5 / 89.9 | 71.1 / 86.6 | 97.1 / 99.0 | 55.2 / 67.5 | 73.6 / 85.7 |
| EMR-Merging | 75.2 / 83.2 | 72.8 / 90.7 | 93.5 / 96.8 | 99.5 / 99.7 | 96.9 / 97.9 | 98.1 / 99.1 | 99.6 / 99.7 | 74.4 / 82.7 | 88.7 / 93.7 |
| + TADrop | 78.7 / 84.3 | 78.6 / 92.1 | 95.2 / 97.4 | 99.4 / 99.7 | 97.4 / 98.1 | 98.7 / 99.1 | 99.7 / 99.8 | 77.9 / 83.5 | 90.7 / 94.2 |

Table 1: Multi-task performance when merging ViT models on eight tasks (a / b: a = ViT-B/32, b = ViT-L/14).

In summary, TADrop is designed as a simple, efficient, and plug-and-play module. It is intended to operate as a key component within the pre-processing operator $\Phi(\cdot)$, focusing specifically on optimizing the critical sparsification step. Due to its self-contained nature, it can be seamlessly integrated into a variety of existing model merging methods as a direct replacement for, or enhancement to, their native sparsification strategies. This allows it to boost their merging performance without introducing additional complexity.

Experiments and Analyses

Setup

Models and Datasets Following the standard setups from prior work (Ilharco et al. 2023; Huang et al. 2024), we evaluated TADrop in three main scenarios: (1) ViT (Vision Tasks): We utilized two vision encoders, ViT-B/32 and ViT-L/14, from the CLIP model (Radford et al. 2021) as pretrained base models. These models were evaluated on eight widely used image classification datasets. (2) GPT-2 (Language Tasks): The GPT-2 model (Radford et al. 2019) was employed for experiments across seven NLP tasks. (3) BEiT3 (Multimodal Tasks): We based on BEiT3-base (Wang et al. 2023) and evaluate it on five challenging multimodal tasks. Detailed dataset names and descriptions evaluated above are in the Appendix.

Baselines As TADrop is a plug-and-play sparsification enhancement module, we primarily validate its benefits by integrating it with three task vector-based merging methods, including: (1) Task Arithmetic (Ilharco et al. 2023): A foundational merging method that merges task vectors through linear summation. (2) Ties-Merging (Yadav et al. 2023): A classic merging method that performs pruning and sign alignment on task vectors before merging. (3) EMR-Merging (Huang et al. 2024): A SOTA merging method that combines a unified model with lightweight task-specific modulators. In addition to the above, we compare the performance of our TADrop-enhanced models against a broader landscape of methods to provide a complete per-

formance picture, including: individual Models, Traditional MTL models, Weight Averaging, Fisher Merging (Matena and Raffel 2022), RegMean (Jin et al. 2023), AdaMerging (Yang et al. 2024b), PCB-Merging (Du et al. 2024), Localize-and-Stitch (He et al. 2025) and ProDistill(Xu, Li, and Zhang 2025). Detailed descriptions of these baselines are provided in the Appendix.

Implementation Details Based on our observations of the parameter distributions, which often resemble skewed normal distributions, we set $a = 0.50$ (the median) and $b = 0.95$ (95th percentile), enabling our metric to quantify the distribution’s heavy-tailedness by measuring the upper tail’s deviation from the center. To further validate this choice, we conducted a hyperparameter sensitivity analysis in the Appendix, which suggests that TADrop remains robust within a reasonable range of values for a and b . Therefore, we use these fixed values across all experiments to demonstrate the method’s out-of-the-box effectiveness without task-specific tuning. When integrated with baseline methods, TADrop is used to replace or enhance their native sparsification steps. The specific integration strategies are as follows: (1) For Task Arithmetic (Ilharco et al. 2023), we apply TADrop as an additional pre-processing operation before the task vectors are aggregated. (2) For Ties-Merging (Yadav et al. 2023), we replace its original pruning step with our TADrop module, while keeping its subsequent sign alignment operations intact. (3) For EMR-Merging (Huang et al. 2024), TADrop computes an adaptive sparsification mask for each tensor, which is then combined with the consensus sign mask by element-wise product.

Results

Performance on ViT models We first validate the effectiveness of TADrop on two Vision Transformer models, ViT-B/32 and ViT-L/14, with the comprehensive results presented in Table 1¹. When integrated with Task Arith-

¹Individual model’s results are from our re-implementation, which are slightly higher than those reported in some prior works.

| Method | CoLA | MNLI | MRPC | QNLI | QQP | RTE | SST2 | Avg. Acc |
|---|-------------|-------------|-------------|-------------|-------------|-------------|-------------|-------------|
| Individul | 76.8 | 82.1 | 80.4 | 88.3 | 89.6 | 65.3 | 91.2 | 82.0 |
| Weight Averaging | 55.0 | 55.1 | 51.0 | 57.6 | 76.7 | 44.8 | 52.5 | 56.1 |
| Fisher Merging (Matena and Raffel 2022) | 54.8 | 58.0 | 39.5 | 63.3 | 81.5 | 49.1 | 64.7 | 58.7 |
| RegMean (Jin et al. 2023) | 61.7 | 70.4 | 65.4 | 69.7 | 78.8 | 56.0 | 79.7 | 68.8 |
| Task Arithmetic (Ilharco et al. 2023) | 68.7 | 68.6 | 69.6 | 70.5 | 81.8 | 47.3 | 83.6 | 70.0 |
| + TADrop | 68.8 | 71.9 | 69.1 | 70.2 | 81.9 | 47.3 | 83.5 | 70.4 |
| Ties-Merging (Yadav et al. 2023) | 68.4 | 71.4 | 68.4 | 69.6 | 82.4 | 47.7 | 81.8 | 70.0 |
| + TADrop | 68.2 | 73.8 | 66.6 | 68.7 | 82.5 | 48.0 | 82.4 | 70.1 |
| EMR-Merging (Huang et al. 2024) | 72.8 | 81.1 | 79.2 | 84.8 | 88.1 | 66.5 | 90.3 | 80.4 |
| + TADrop | 73.8 | 81.2 | 80.1 | 87.8 | 88.8 | 66.4 | 90.4 | 81.2 |

Table 2: Multi-task performance when merging GPT-2 models on seven text classification tasks.

| Methods | COCO-Re | | COCO-Captioning | | | ImageNet | NLVR2 | VQAv2 |
|---------------------------------|-------------|-------------|-----------------|-------------|-------------|-------------|-------------|-------------|
| | Acc | BLEU | CIDEr | METEOR | ROUGE | | | |
| Individual | 84.6 | 39.4 | 1.34 | 31.1 | 60.1 | 85.4 | 77.7 | 84.4 |
| EMR-Merging (Huang et al. 2024) | 79.5 | 28.9 | 1.06 | 27.2 | 53.4 | 77.4 | 74.8 | 72.1 |
| + TADrop | 80.9 | 33.8 | 1.18 | 28.6 | 56.2 | 80.1 | 77.4 | 72.1 |

Table 3: Performance of merging multi-modal BEiT3 models on five vision-language tasks.

metric, TADrop boosts the average accuracy by 0.9% on ViT-B/32 and 0.4% on ViT-L/14. When applied to Ties-Merging, which already incorporates a complex, multi-stage sparsification process, the additional gains are marginal. This suggests that the primary benefits of pruning have been largely captured by the baseline itself, leaving less room for improvement. Most notably, TADrop demonstrates its full potential when enhancing EMR-Merging. Here, TADrop achieves a remarkable 2.0% and 0.5% absolute performance gain on the ViT-B/32 and ViT-L/14 model, respectively. As a result, the EMR-Merging + TADrop model surpasses all other merging baselines, establishing a new SOTA for this experimental setup. Furthermore, this superior performance is not limited to an 8-task scenario; as detailed in Figure 4 and Appendix, TADrop continues to deliver substantial improvements when scaled to a more challenging set of 30 tasks, further validating its effectiveness and robustness.

Performance on GPT-2 models To validate the generalizability of TADrop from the vision domain to NLP, we conducted further experiments on merging models based on GPT-2 across seven tasks from GLUE (Wang et al. 2018). As shown in Table 2, the results demonstrate that TADrop’s adaptive sparsification strategy is equally applicable to language models and can yield performance improvements for existing merging methods. Specifically, it improves the average accuracy of Task Arithmetic by 0.4%, Ties-Merging by 0.1%, and the EMR-Merging by 0.8%. The results confirm that TADrop not only performs exceptionally on vision models but also serves as a universal enhancement module that boosts the performance of language models.

Performance on BEiT models To further investigate the generalization capability of TADrop in more complex scenarios, we conducted merging experiments on the multi-modal model, BEiT3, across five vision-language tasks. It is worth noting that in our preliminary experiments, many classic merging methods (e.g., Weight Averaging, Task Arithmetic, Ties-Merging) performed poorly on the complex generation task of COCO-Captioning, yielding results that were not meaningful. Therefore, we focus our comparison on EMR-Merging. As presented in Table 3, the results demonstrate that TADrop delivers comprehensive and significant performance improvements. In the COCO-Re and ImageNet classification tasks, TADrop brings absolute accuracy gains of 1.4% and 2.7%, respectively. On the more challenging COCO-Captioning task, TADrop also achieves improvements across all four metrics. These confirm that TADrop is a versatile strategy, successfully extending beyond unimodal classification to complex, multimodal generation tasks.

Analyses

Performance of TADrop in many-task merging scenario A critical test for any merging method is its robustness against the escalating parameter interference that occurs as the number of tasks increases. To evaluate TADrop’s ability to mitigate this challenge, we conducted a scalability experiment on the ViT-B/16 model, progressively increasing the number of merged tasks from 8 to 30 and observing its effect on the EMR-Merging baseline. As illustrated in Figure 4, the performance gain delivered by TADrop over the EMR-Merging baseline (the light blue shaded area) not only remains stable but actually widens as more tasks are added.

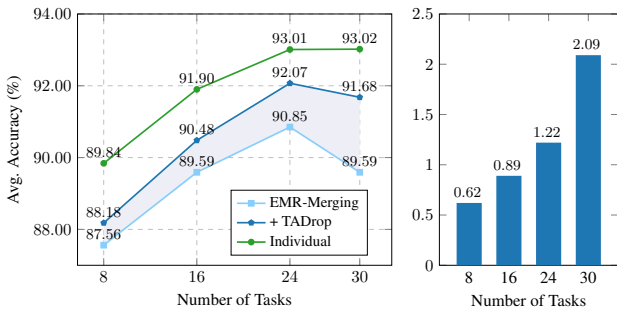


Figure 4: Robustness and scalability of TADrop in large-scale merging. Left: Absolute average accuracy of baselines. Right: Absolute performance gain of TADrop over the EMR-Merging.

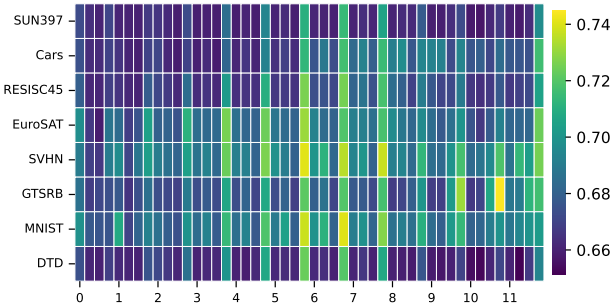


Figure 5: Inter-Task adaptivity of sparsity rates.

For instance, the performance advantage grows from 0.62% with 8 tasks to 1.22% with 24 tasks, and reaches a substantial 2.09% with 30 tasks. This trend indicates that TADrop’s adaptive sparsification mechanism is effectively counteracting the escalating parameter conflict. This finding confirms that TADrop is not merely a technique effective for a few tasks, but a robust and scalable strategy well-suited for the challenges of more realistic, many-task merging scenarios.

Adaptive sparsity rates To provide a mechanistic explanation for TADrop’s effectiveness and to visually demonstrate how it addresses parameter heterogeneity, we visualize the adaptive sparsity rates it computes. The Figure 5

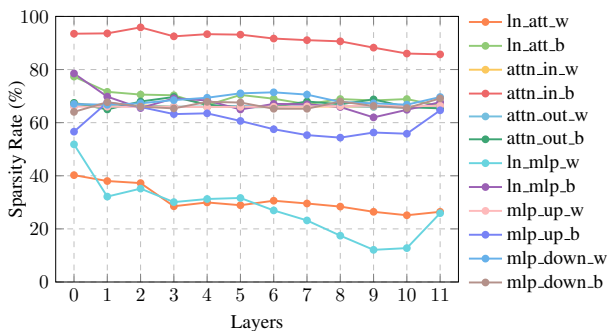


Figure 6: Intra-Model adaptivity of sparsity rates.

| Model | Avg. Acc |
|---------------------------------|----------|
| EMR-Merging (Huang et al. 2024) | 88.7 |
| W/ Global Sparsification | 89.9 |
| W/o Scale | 86.8 |
| 1 – d Scale | 71.1 |
| TADrop | 90.7 |

Table 4: Ablation study results on the 8 ViT tasks.

provides a macroscopic view, visualizing the task-specific sparsity patterns that result from TADrop’s adaptive mechanism. It reveals a highly non-uniform sparsification “landscape”, which stands in stark contrast to the “one-size-fits-all” strategy of existing methods (e.g., Ties-Merging, which defaults to a fixed 80% sparsity rate). The fact that TADrop assigns vastly different sparsification patterns to different tasks validates our core premise. The Figure 6 offers a microscopic perspective on TADrop’s intra-model adaptivity within a single task (SUN397), revealing that different component types are treated with distinct sparsity rates. Most interestingly, we find that this intra-model sparsification pattern is strikingly consistent across tasks (see Appendix), suggesting that different parameter types play distinct, intrinsic roles during fine-tuning. The success of TADrop lies in its ability to automatically discover and exploit this underlying structural pattern, enabling a more precise and effective sparsification than the fixed-rate method.

Ablation study To dissect the contribution of each component in TADrop, we conducted an ablation study using EMR-Merging (88.7%) as the baseline, with results presented in Table 4. The full TADrop method achieves the top performance at 90.7%. Our analysis reveals that both of its components are essential: (1) Removing the norm-preserving scaling step (W/o Scale) is detrimental, causing performance to collapse to 86.8%. This highlights its critical role in stabilizing the merge after pruning. (2) Replacing our adaptive strategy with a simpler Global Sparsification is beneficial, reaching 89.9%, but it still falls short of the full method’s performance. This confirms the value added by the adaptive, fine-grained nature of our approach. This demonstrates that TADrop’s success stems from the indispensable synergy between its two core components: an adaptive strategy to accurately identify redundancy and a scaling mechanism to realize the full performance gains.

Conclusion

In this work, we addressed the limitation of “one-size-fits-all” sparsification in model merging. We identified and empirically demonstrated that parameter heterogeneity is an intrinsic property of task vectors, and that ignoring the model’s structural hierarchy forces a suboptimal trade-off between information preservation and redundancy removal. To resolve this, we proposed TADrop, a simple, plug-and-play, tensor-wise adaptive drop strategy. By leveraging the distributional properties of each tensor to dynamically as-

sign a tailored drop rate, TADrop resolves the suboptimal trade-offs of global approaches, removing redundancy while preserving critical information. Our extensive experiments across vision, language, and multimodal tasks confirmed the effectiveness and generality of TADrop. When integrated with SOTA methods, it consistently delivered significant performance gains, establishing a new SOTA. This work underscores the importance of structurally-aware merging techniques and establishes TADrop as an effective, robust method for the challenge of parameter heterogeneity.

References

Ahmed, M. I.; Mamun, S. M.; and Asif, A. U. Z. 2021. Dcnn-based vegetable image classification using transfer learning: A comparative study. In *2021 5th International Conference on Computer, Communication and Signal Processing (ICCCSP)*, 235–243. IEEE.

Ahmed, S. I.; Ibrahim, M.; Nadim, M.; Rahman, M. M.; Shejunti, M. M.; Jabid, T.; and Ali, M. S. 2023. MangoLeafBD: A comprehensive image dataset to classify diseased and healthy mango leaves. *Data in Brief*, 47: 108941.

Bansal, P. 2019. Intel image classification. Available on <https://www.kaggle.com/puneet6060/intel-image-classification>, *Online*.

Bossard, L.; Guillaumin, M.; and Van Gool, L. 2014. Food-101 – Mining Discriminative Components with Random Forests. In *European Conference on Computer Vision*.

Caruana, R. 1997. Multitask Learning. *Mach. Learn.*, 28(1): 41–75.

CCHANG. 2018. Garbage Classification. <https://www.kaggle.com/ds/81794>.

Chang, K.; Xu, S.; Wang, C.; Luo, Y.; Xiao, T.; and Zhu, J. 2024. Efficient Prompting Methods for Large Language Models: A Survey. *CoRR*, abs/2404.01077.

Cheng, G.; Han, J.; and Lu, X. 2017. Remote Sensing Image Scene Classification: Benchmark and State of the Art. *Proc. IEEE*, 105(10): 1865–1883.

Chopra, H.; Rambhia, V.; and Adve, V. 2025. LEWIS (LayEr WIse Sparsity)–A Training Free Guided Model Merging Approach. *arXiv preprint arXiv:2503.03874*.

Cimpoi, M.; Maji, S.; Kokkinos, I.; Mohamed, S.; and Vedaldi, A. 2014. Describing Textures in the Wild. In *2014 IEEE Conference on Computer Vision and Pattern Recognition, CVPR 2014, Columbus, OH, USA, June 23-28, 2014*, 3606–3613. IEEE Computer Society.

Coates, A.; Ng, A.; and Lee, H. 2011. An analysis of single-layer networks in unsupervised feature learning. In *Proceedings of the fourteenth international conference on artificial intelligence and statistics*, 215–223. JMLR Workshop and Conference Proceedings.

Cohen, G.; Afshar, S.; Tapson, J.; and Van Schaik, A. 2017. EMNIST: Extending MNIST to handwritten letters. In *2017 international joint conference on neural networks (IJCNN)*, 2921–2926. IEEE.

Cukierski, W. ???? Dogs vs. cats, 2013. URL <https://kaggle.com/competitions/dogs-vs-cats>.

Deep, P. T.; Bhardwaj, R.; and Poria, S. 2024. DELLA-Merging: Reducing Interference in Model Merging through Magnitude-Based Sampling. *CoRR*, abs/2406.11617.

DeepNets. ???? Landscape Recognition. <https://www.kaggle.com/datasets/utkarshsaxenadn/landscape-recognition-image-dataset-12k-images>.

Deng, J.; Dong, W.; Socher, R.; Li, L.; Li, K.; and Fei-Fei, L. 2009. ImageNet: A large-scale hierarchical image database. In *2009 IEEE Computer Society Conference on Computer Vision and Pattern Recognition (CVPR 2009), 20-25 June 2009, Miami, Florida, USA*, 248–255. IEEE Computer Society.

Devlin, J.; Chang, M.; Lee, K.; and Toutanova, K. 2019. BERT: Pre-training of Deep Bidirectional Transformers for Language Understanding. In *Proceedings of the 2019 Conference of the North American Chapter of the Association for Computational Linguistics: Human Language Technologies, NAACL-HLT 2019, Minneapolis, MN, USA, June 2-7, 2019, Volume 1 (Long and Short Papers)*, 4171–4186.

Dolan, W. B.; and Brockett, C. 2005. Automatically Constructing a Corpus of Sentential Paraphrases. In *Proceedings of the Third International Workshop on Paraphrasing, IWP@IJCNLP 2005, Jeju Island, Korea, October 2005, 2005*. Asian Federation of Natural Language Processing.

Dosovitskiy, A.; Beyer, L.; Kolesnikov, A.; Weissenborn, D.; Zhai, X.; Unterthiner, T.; Dehghani, M.; Minderer, M.; Heigold, G.; Gelly, S.; Uszkoreit, J.; and Houlsby, N. 2021. An Image is Worth 16x16 Words: Transformers for Image Recognition at Scale. In *9th International Conference on Learning Representations, ICLR 2021, Virtual Event, Austria, May 3-7, 2021*.

Du, G.; Lee, J.; Li, J.; Jiang, R.; Guo, Y.; Yu, S.; Liu, H.; Goh, S. K.; Tang, H.; He, D.; and Zhang, M. 2024. Parameter Competition Balancing for Model Merging. In *Advances in Neural Information Processing Systems 38: Annual Conference on Neural Information Processing Systems 2024, NeurIPS 2024, Vancouver, BC, Canada, December 10 - 15, 2024*.

Fisher, R. A. 1922. On the mathematical foundations of theoretical statistics. *Philosophical transactions of the Royal Society of London. Series A, containing papers of a mathematical or physical character*, 222(594-604): 309–368.

Giampiccolo, D.; Magnini, B.; Dagan, I.; and Dolan, B. 2007. The Third PASCAL Recognizing Textual Entailment Challenge. In Sekine, S.; Inui, K.; Dagan, I.; Dolan, B.; Giampiccolo, D.; and Magnini, B., eds., *Proceedings of the ACL-PASCAL@ACL 2007 Workshop on Textual Entailment and Paraphrasing, Prague, Czech Republic, June 28-29, 2007*, 1–9. Association for Computational Linguistics.

Goyal, Y.; Khot, T.; Summers-Stay, D.; Batra, D.; and Parikh, D. 2017. Making the V in VQA Matter: Elevating the Role of Image Understanding in Visual Question Answering. In *2017 IEEE Conference on Computer Vision and Pattern Recognition, CVPR 2017, Honolulu, HI, USA, July 21-26, 2017*, 6325–6334. IEEE Computer Society.

He, Y.; Hu, Y.; Lin, Y.; Zhang, T.; and Zhao, H. 2025.

Localize-and-Stitch: Efficient Model Merging via Sparse Task Arithmetic. *Trans. Mach. Learn. Res.*, 2025.

Helber, P.; Bischke, B.; Dengel, A.; and Borth, D. 2019. EuroSAT: A Novel Dataset and Deep Learning Benchmark for Land Use and Land Cover Classification. *IEEE J. Sel. Top. Appl. Earth Obs. Remote. Sens.*, 12(7): 2217–2226.

Huang, C.; Ye, P.; Chen, T.; He, T.; Yue, X.; and Ouyang, W. 2024. EMR-Merging: Tuning-Free High-Performance Model Merging. In *Advances in Neural Information Processing Systems 38: Annual Conference on Neural Information Processing Systems 2024, NeurIPS 2024, Vancouver, BC, Canada, December 10 - 15, 2024*.

Ilharco, G.; Ribeiro, M. T.; Wortsman, M.; Schmidt, L.; Hajishirzi, H.; and Farhadi, A. 2023. Editing models with task arithmetic. In *The Eleventh International Conference on Learning Representations, ICLR 2023, Kigali, Rwanda, May 1-5, 2023*.

Iyer, S.; Dandekar, N.; Csernai, K.; et al. 2017. First quora dataset release: Question pairs. *data. quora. com*.

Jalal, M.; Wang, K.; Jefferson, S.; Zheng, Y.; Nsoesie, E. O.; and Betke, M. 2019. Scraping social media photos posted in Kenya and elsewhere to detect and analyze food types. In *Proceedings of the 5th International Workshop on Multimedia Assisted Dietary Management*, 50–59.

Jin, X.; Ren, X.; Preotiuc-Pietro, D.; and Cheng, P. 2023. Dataless Knowledge Fusion by Merging Weights of Language Models. In *The Eleventh International Conference on Learning Representations, ICLR 2023, Kigali, Rwanda, May 1-5, 2023*. OpenReview.net.

Khosla, A.; Jayadevaprakash, N.; Yao, B.; and Fei-Fei, L. 2011. Novel Dataset for Fine-Grained Image Categorization. In *First Workshop on Fine-Grained Visual Categorization, IEEE Conference on Computer Vision and Pattern Recognition*. Colorado Springs, CO.

Kolesnikov, A.; Beyer, L.; Zhai, X.; Puigcerver, J.; Yung, J.; Gelly, S.; and Houlsby, N. 2019. Big Transfer (BiT): General Visual Representation Learning. *arXiv preprint arXiv:1912.11370*.

Krause, J.; Stark, M.; Deng, J.; and Fei-Fei, L. 2013. 3D Object Representations for Fine-Grained Categorization. In *2013 IEEE International Conference on Computer Vision Workshops, ICCV Workshops 2013, Sydney, Australia, December 1-8, 2013*, 554–561. IEEE Computer Society.

Krizhevsky, A.; Hinton, G.; et al. 2009. Learning multiple layers of features from tiny images.

Lab, M. A. 2020. Bean disease dataset.

LeCun, Y. 1998. The MNIST database of handwritten digits. <http://yann.lecun.com/exdb/mnist/>.

Lee, C.; Choi, J.; Lee, C.; Kim, D.; and Hong, S. 2025. AdaRank: Adaptive Rank Pruning for Enhanced Model Merging. *CoRR*, abs/2503.22178.

Lin, T.; Maire, M.; Belongie, S. J.; Hays, J.; Perona, P.; Ramanan, D.; Dollár, P.; and Zitnick, C. L. 2014. Microsoft COCO: Common Objects in Context. In Fleet, D. J.; Pajdla, T.; Schiele, B.; and Tuytelaars, T., eds., *Computer Vision - ECCV 2014 - 13th European Conference, Zurich, Switzerland, September 6-12, 2014, Proceedings, Part V*, volume 8693 of *Lecture Notes in Computer Science*, 740–755. Springer.

Lu, Z.; Fan, C.; Wei, W.; Qu, X.; Chen, D.; and Cheng, Y. 2024. Twin-Merging: Dynamic Integration of Modular Expertise in Model Merging. In *Advances in Neural Information Processing Systems 38: Annual Conference on Neural Information Processing Systems 2024, NeurIPS 2024, Vancouver, BC, Canada, December 10 - 15, 2024*.

Luo, Y.; Zheng, T.; Mu, Y.; Li, B.; Zhang, Q.; Gao, Y.; Xu, Z.; Feng, P.; Liu, X.; Xiao, T.; and Zhu, J. 2025. Beyond Decoder-only: Large Language Models Can be Good Encoders for Machine Translation. In *Findings of the Association for Computational Linguistics, ACL 2025, Vienna, Austria, July 27 - August 1, 2025*, 9399–9431.

Mamaev, A. ???? Flowers Recognition. <https://www.kaggle.com/datasets/alxmamaev/flowers-recognition>.

Matena, M.; and Raffel, C. 2022. Merging Models with Fisher-Weighted Averaging. In *Advances in Neural Information Processing Systems 35: Annual Conference on Neural Information Processing Systems 2022, NeurIPS 2022, New Orleans, LA, USA, November 28 - December 9, 2022*.

Muresan, H.; and Oltean, M. 2018. Fruit recognition from images using deep learning. *Acta Universitatis Sapientiae, Informatica*, 10(1): 26–42.

Parkhi, O. M.; Vedaldi, A.; Zisserman, A.; and Jawahar, C. 2012. Cats and dogs. In *2012 IEEE conference on computer vision and pattern recognition*, 3498–3505. IEEE.

Pogorelov, K.; Randel, K. R.; Griwodz, C.; Eskeland, S. L.; de Lange, T.; Johansen, D.; Spampinato, C.; Dang-Nguyen, D.-T.; Lux, M.; Schmidt, P. T.; et al. 2017. Kvasir: A multi-class image dataset for computer aided gastrointestinal disease detection. In *Proceedings of the 8th ACM on Multimedia Systems Conference*, 164–169.

Radford, A.; Kim, J. W.; Hallacy, C.; Ramesh, A.; Goh, G.; Agarwal, S.; Sastry, G.; Askell, A.; Mishkin, P.; Clark, J.; Krueger, G.; and Sutskever, I. 2021. Learning Transferable Visual Models From Natural Language Supervision. In *Proceedings of the 38th International Conference on Machine Learning, ICML 2021, 18-24 July 2021, Virtual Event*, 8748–8763.

Radford, A.; and Narasimhan, K. 2018. Improving Language Understanding by Generative Pre-Training.

Radford, A.; Wu, J.; Child, R.; Luan, D.; Amodei, D.; and Sutskever, I. 2019. Language Models are Unsupervised Multitask Learners.

Raffel, C.; Shazeer, N.; Roberts, A.; Lee, K.; Narang, S.; Matena, M.; Zhou, Y.; Li, W.; and Liu, P. J. 2020. Exploring the Limits of Transfer Learning with a Unified Text-to-Text Transformer. *J. Mach. Learn. Res.*, 21: 140:1–140:67.

Rajpurkar, P.; Zhang, J.; Lopyrev, K.; and Liang, P. 2016. SQuAD: 100, 000+ Questions for Machine Comprehension of Text. In Su, J.; Carreras, X.; and Duh, K., eds., *Proceedings of the 2016 Conference on Empirical Methods in Natural Language Processing, EMNLP 2016, Austin, Texas, USA, November 1-4, 2016*, 2383–2392. The Association for Computational Linguistics.

Sanh, V.; Webson, A.; Raffel, C.; Bach, S. H.; Sutawika, L.; Alyafeai, Z.; Chaffin, A.; Stiegler, A.; Raja, A.; Dey, M.; Bari, M. S.; Xu, C.; Thakker, U.; Sharma, S. S.; Szczechla, E.; Kim, T.; Chhablani, G.; Nayak, N. V.; Datta, D.; Chang, J.; Jiang, M. T.; Wang, H.; Manica, M.; Shen, S.; Yong, Z. X.; Pandey, H.; Bawden, R.; Wang, T.; Neeraj, T.; Rozen, J.; Sharma, A.; Santilli, A.; Févry, T.; Fries, J. A.; Teehan, R.; Scao, T. L.; Biderman, S.; Gao, L.; Wolf, T.; and Rush, A. M. 2022. Multitask Prompted Training Enables Zero-Shot Task Generalization. In *ICLR*. OpenReview.net.

Socher, R.; Perelygin, A.; Wu, J.; Chuang, J.; Manning, C. D.; Ng, A. Y.; and Potts, C. 2013. Recursive Deep Models for Semantic Compositionality Over a Sentiment Treebank. In *Proceedings of the 2013 Conference on Empirical Methods in Natural Language Processing, EMNLP 2013, 18-21 October 2013, Grand Hyatt Seattle, Seattle, Washington, USA, A meeting of SIGDAT, a Special Interest Group of the ACL*, 1631–1642. ACL.

Song, H.; Kim, M.; and Lee, J.-G. 2019. Selfie: Refurbishing unclean samples for robust deep learning. In *International conference on machine learning*, 5907–5915. PMLR.

Stallkamp, J.; Schlipsing, M.; Salmen, J.; and Igel, C. 2011. The German Traffic Sign Recognition Benchmark: A multi-class classification competition. In *The 2011 International Joint Conference on Neural Networks, IJCNN 2011, San Jose, California, USA, July 31 - August 5, 2011*, 1453–1460. IEEE.

Suhr, A.; Zhou, S.; Zhang, A.; Zhang, I.; Bai, H.; and Artzi, Y. 2019. A Corpus for Reasoning about Natural Language Grounded in Photographs. In Korhonen, A.; Traum, D. R.; and Márquez, L., eds., *Proceedings of the 57th Conference of the Association for Computational Linguistics, ACL 2019, Florence, Italy, July 28- August 2, 2019, Volume 1: Long Papers*, 6418–6428. Association for Computational Linguistics.

Wah, C.; Branson, S.; Welinder, P.; Perona, P.; and Belongie, S. 2011. The caltech-ucsd birds-200-2011 dataset.

Wang, A.; Singh, A.; Michael, J.; Hill, F.; Levy, O.; and Bowman, S. R. 2018. GLUE: A multi-task benchmark and analysis platform for natural language understanding. *arXiv preprint arXiv:1804.07461*.

Wang, K.; Dimitriadis, N.; Ortiz-Jiménez, G.; Fleuret, F.; and Frossard, P. 2024. Localizing Task Information for Improved Model Merging and Compression. In *Forty-first International Conference on Machine Learning, ICML 2024, Vienna, Austria, July 21-27, 2024*.

Wang, W.; Bao, H.; Dong, L.; Bjorck, J.; Peng, Z.; Liu, Q.; Aggarwal, K.; Mohammed, O. K.; Singhal, S.; Som, S.; and Wei, F. 2023. Image as a Foreign Language: BEIT Pretraining for Vision and Vision-Language Tasks. In *IEEE/CVF Conference on Computer Vision and Pattern Recognition, CVPR 2023, Vancouver, BC, Canada, June 17-24, 2023*, 19175–19186.

Warstadt, A.; Singh, A.; and Bowman, S. R. 2019. Neural network acceptability judgments. *Transactions of the Association for Computational Linguistics*, 7: 625–641.

Williams, A.; Nangia, N.; and Bowman, S. R. 2017. A broad-coverage challenge corpus for sentence understanding through inference. *arXiv preprint arXiv:1704.05426*.

Wortsman, M.; Ilharco, G.; Gadre, S. Y.; Roelofs, R.; Lopes, R. G.; Morcos, A. S.; Namkoong, H.; Farhadi, A.; Carmon, Y.; Kornblith, S.; and Schmidt, L. 2022. Model soups: averaging weights of multiple fine-tuned models improves accuracy without increasing inference time. In *International Conference on Machine Learning, ICML 2022, 17-23 July 2022, Baltimore, Maryland, USA*, 23965–23998.

Xiao, H.; Rasul, K.; and Vollgraf, R. 2017. Fashion-mnist: a novel image dataset for benchmarking machine learning algorithms. *arXiv preprint arXiv:1708.07747*.

Xiao, H.; Zhang, F.; Shen, Z.; Wu, K.; and Zhang, J. 2021. Classification of weather phenomenon from images by using deep convolutional neural network. *Earth and Space Science*, 8(5): e2020EA001604.

Xiao, J.; Ehinger, K. A.; Hays, J.; Torralba, A.; and Oliva, A. 2016. SUN Database: Exploring a Large Collection of Scene Categories. *Int. J. Comput. Vis.*, 119(1): 3–22.

Xiao, T.; and Zhu, J. 2025. Foundations of Large Language Models. *arXiv preprint arXiv:2501.09223*.

Xu, J.; Li, J.; and Zhang, J. 2025. Scalable Model Merging with Progressive Layer-wise Distillation. *CoRR*, abs/2502.12706.

Yadav, P.; Tam, D.; Choshen, L.; Raffel, C. A.; and Bansal, M. 2023. TIES-Merging: Resolving Interference When Merging Models. In *Advances in Neural Information Processing Systems 36: Annual Conference on Neural Information Processing Systems 2023, NeurIPS 2023, New Orleans, LA, USA, December 10 - 16, 2023*.

Yang, E.; Shen, L.; Guo, G.; Wang, X.; Cao, X.; Zhang, J.; and Tao, D. 2024a. Model Merging in LLMs, MLLMs, and Beyond: Methods, Theories, Applications and Opportunities. *arXiv:2408.07666*.

Yang, E.; Wang, Z.; Shen, L.; Liu, S.; Guo, G.; Wang, X.; and Tao, D. 2024b. AdaMerging: Adaptive Model Merging for Multi-Task Learning. In *The Twelfth International Conference on Learning Representations, ICLR 2024, Vienna, Austria, May 7-11, 2024*.

Yang, Y.; Li, Y.; Wang, H.; Wei, X.; Yu, J. J.; Chen, Y.; and Chen, G. 2025a. ImPart: Importance-Aware Delta-Sparsification for Improved Model Compression and Merging in LLMs. In *Proceedings of the 63rd Annual Meeting of the Association for Computational Linguistics (Volume 1: Long Papers)*, ACL 2025, Vienna, Austria, July 27 - August 1, 2025, 18817–18829.

Yang, Z.; Qi, B.; Sun, H.; Long, W.; Zhao, R.; and Gao, X. 2025b. CABS: Conflict-Aware and Balanced Sparsification for Enhancing Model Merging. *CoRR*, abs/2503.01874.

Yu, L.; Yu, B.; Yu, H.; Huang, F.; and Li, Y. 2024. Language Models are Super Mario: Absorbing Abilities from Homologous Models as a Free Lunch. In *Forty-first International Conference on Machine Learning, ICML 2024, Vienna, Austria, July 21-27, 2024*.

Yu, T.; Kumar, S.; Gupta, A.; Levine, S.; Hausman, K.; and Finn, C. 2020. Gradient Surgery for Multi-Task Learning. In *Advances in Neural Information Processing Systems 33: Annual Conference on Neural Information Processing Systems 2020, NeurIPS 2020, December 6-12, 2020, virtual*.

Yuval, N. 2011. Reading digits in natural images with unsupervised feature learning. In *NIPS Workshop on Deep Learning and Unsupervised Feature Learning*.

Zhang, B.; Li, H.; Shi, C.; Rong, G.; Zhao, H.; Wang, D.; Guo, D.; and Wang, M. 2025. Merging Smarter, Generalizing Better: Enhancing Model Merging on OOD Data. *CoRR*, abs/2506.09093.

Zhang, Y.; and Yang, Q. 2022. A Survey on Multi-Task Learning. *IEEE Trans. Knowl. Data Eng.*, 34(12): 5586–5609.

A. Evaluated Datasets

We evaluate our models on a wide range of datasets, including image classification datasets, GLUE benchmark, and BEiT dataset

Image Classification Datasets (for Vit Model)

- **SUN397** (Xiao et al. 2016): A scene classification dataset with 397 categories and over 108,000 images, covering diverse indoor and outdoor environments.
- **Stanford Cars** (Krause et al. 2013): A fine-grained vehicle classification dataset with 196 car models and 16,185 images categorized by make, model, and year.
- **RESISC45** (Cheng, Han, and Lu 2017): A remote sensing scene classification dataset with 45 categories and 31,500 images, including airports, residential areas, and ports.
- **EuroSAT** (Helber et al. 2019): A land cover classification dataset with 10 categories and 27,000 satellite images derived from Sentinel-2 data.
- **SVHN** (Yuval 2011): A digit recognition dataset with over 600,000 street view images of house numbers in natural scenes.
- **GTSRB** (Stallkamp et al. 2011): A traffic sign classification benchmark with 43 categories and more than 50,000 images collected in real-world conditions.
- **MNIST** (LeCun 1998): A classic handwritten digit dataset with 70,000 grayscale images across 10 digit classes.
- **DTD** (Cimpoi et al. 2014): A texture classification dataset with 47 describable visual texture attributes and around 5,640 images.
- **CIFAR-10** (Krizhevsky, Hinton et al. 2009): Consists of 60,000 32x32 color images in 10 classes, with 6,000 images per class, commonly used for image recognition tasks.
- **Vegetables** (Ahmed, Mamun, and Asif 2021): An image dataset containing 15,000 images of 15 different types of vegetables for classification tasks.
- **Food-101** (Bossard, Guillaumin, and Van Gool 2014): A challenging dataset of 101,000 images representing 101 different food categories, designed for food recognition.
- **Kvasir-v2** (Pogorelov et al. 2017): A dataset of images from inside the gastrointestinal tract, containing different anatomical landmarks and pathological findings.
- **Intel Images** (Bansal 2019): A dataset of around 25,000 images of natural scenes from around the world, classified into 6 categories (buildings, forest, glacier, mountain, sea, and street).
- **Weather** (Xiao et al. 2021): Contains 1125 images categorized into four weather types: sunrise, shine, rainy, and cloudy, for weather classification.
- **Cats and dogs** (Cukierski): A classic computer vision dataset from a Kaggle competition containing over 25,000 images of cats and dogs for binary classification.

- **MangoLeafBD** (Ahmed et al. 2023): A dataset of 4,000 images depicting 7 different diseases affecting mango leaves, aimed at aiding agricultural disease detection.
- **Beans** (Lab 2020): A dataset of bean leaf images with three classes: two disease classes (Angular Leaf Spot and Bean Rust) and a healthy class.
- **CIFAR-100** (Krizhevsky, Hinton et al. 2009): Similar to CIFAR-10, this dataset has 60,000 32x32 color images but is divided into 100 classes, with 600 images per class.
- **Dogs** (Khosla et al. 2011): The Stanford Dogs dataset contains 20,580 images of 120 breeds of dogs from around the world and is built for fine-grained image categorization.
- **Fashion MNIST** (Xiao, Rasul, and Vollgraf 2017): A dataset of 70,000 grayscale images of 10 types of fashion articles from Zalando, serving as a direct drop-in replacement for the original MNIST.
- **Oxford-IIIT-Pet** (Parkhi et al. 2012): A large dataset of 37 pet categories with roughly 200 images for each class, featuring varied scales, poses, and lighting.
- **Landscape Recognition** (DeepNets): A collection of over 12,000 images for landscape recognition, categorized into predicaments like desolate, mountains, and glaciers.
- **Flowers Recognition** (Mamaev): A dataset for flower recognition, containing over 4,000 images of various flower species.
- **STL-10** (Coates, Ng, and Lee 2011): An image recognition dataset inspired by CIFAR-10, but with a smaller number of labeled training examples and a larger number of unlabeled examples for semi-supervised learning.
- **CUB-200-2011** (Wah et al. 2011): The Caltech-UCSD Birds-200-2011 is a challenging dataset containing 11,788 images of 200 bird species, used for fine-grained visual categorization.
- **EMNIST** (Cohen et al. 2017): The Extended MNIST dataset is a set of handwritten character digits derived from the NIST Special Database 19, containing both digits and letters.
- **KenyanFood13** (Jalal et al. 2019): A dataset containing over 16,000 images of 13 different types of common Kenyan foods for classification.
- **Animal-10N** (Song, Kim, and Lee 2019): A dataset of 10 animal categories with 55,000 images, specifically designed with real-world label noise to facilitate the study of learning with noisy labels.
- **Garbage Classification** (CCHANG 2018): A dataset of 2,527 images classified into six categories of garbage (glass, paper, cardboard, plastic, metal, and trash) for waste classification systems.
- **Fruits-360** (Muresan and Oltean 2018): A dataset with over 90,000 images of 131 types of fruits and vegetables, captured with consistent lighting and background to focus on object recognition.

GLUE Benchmark (for GPT-2 Model)

- **CoLA** (Warstadt, Singh, and Bowman 2019): Linguistic acceptability classification with $\sim 10k$ sentences labeled as acceptable or unacceptable.
- **SST-2** (Socher et al. 2013): Sentiment analysis with $\sim 70k$ movie review sentences labeled as positive or negative.
- **MRPC** (Dolan and Brockett 2005): Paraphrase detection with $\sim 5.8k$ sentence pairs labeled as semantically equivalent or not.
- **QQP** (Iyer et al. 2017): Large-scale paraphrase identification with over 400k Quora question pairs labeled as duplicate or not.
- **MNLI** (Williams, Nangia, and Bowman 2017): Natural language inference with 393k sentence pairs labeled as entailment, contradiction, or neutral.
- **QNLI** (Rajpurkar et al. 2016): Question answering converted to binary entailment classification, with 105k question-context pairs.
- **RTE** (Giampiccolo et al. 2007): Textual entailment classification with $\sim 2.5k$ sentence pairs from previous RTE challenges.

Multimodal Datasets (for BEiT Model)

- **ImageNet-1k** (Deng et al. 2009): Image classification with 1.2M training images across 1,000 object categories.
- **VQAv2** (Goyal et al. 2017): Visual question answering with 1.1M image-question-answer triplets from 200k images.
- **NLVR2** (Suhr et al. 2019): Visual reasoning over image pairs with 100k sentence-image pairs labeled for binary consistency.
- **COCO Captioning** (Lin et al. 2014): Image captioning dataset with over 120k images, each paired with five human-written captions.
- **COCO Retrieval** (Lin et al. 2014): Cross-modal retrieval dataset supporting both image-to-text and text-to-image tasks using COCO images and captions.

B. Baseline Details

This section provides a detailed baseline description. Our experiments encompass seven comparison methods:

- **Individual** means that each task uses an independent fine-tuned model, which has no interference between tasks, but cannot perform multiple tasks simultaneously.
- **Traditional MTL** collects the original training data of all tasks together to train a multi-task model. It can be used as a reference *upper bound* for model merging work.
- **Weight Averaging** is the simplest method of model merging, which directly averages the parameters of multiple models using $\theta_m = \sum_{t=1}^n \theta_t / n$, calculating the element-wise mean of all individual models. It can be used as a *lower bound* for model merging. (Wortsman et al. 2022).

- **Fisher Merging** (Matena and Raffel 2022) calculates the Fisher information matrix (Fisher 1922) $\hat{F}_t = \mathbb{E}_{x \sim D_t} \mathbb{E}_{y \sim p_{\theta_t}(y|x)} \nabla_{\theta_t} (\log p_{\theta_t}(y|x_t))^2$ to measure the importance of each parameter when merging models for task t , where model merging is performed according to the guidance of this importance.
- **RegMean** (Jin et al. 2023) imposes a constraint when merging models, that is, the L_2 distance between the merged model's and the individual models' activations. It computes a least-squares solution as $\theta_m = (\sum_{t=1}^n X_t^T X_t)^{-1} \sum_{t=1}^n (X_t^T X_t \theta_t)$, where X_t is the input activation of the corresponding layer.
- **Task Arithmetic** (Ilharco et al. 2023) first defines the concept of “task vectors” and merges these vectors into a pre-trained model to execute multi-task learning. The model is produced by scaling and adding the task vectors to the initial model as $\theta_m = \theta_{\text{init}} + \lambda * \sum_{t=1}^n \tau_t$.
- **Ties-Merging** (Yadav et al. 2023) further solves the task conflict problem in Task Arithmetic (Ilharco et al. 2023). It eliminates redundant parameters and resolves symbol conflicts through three steps: Trim, Elect Sign, and Disjoint Merge.
- **EMR-Merging** (Huang et al. 2024) creates a unified task vector, τ_{uni} , by electing a dominant sign and maximum magnitude from all task vectors. For inference on a specific task t , it generates a model on-the-fly by modulating this unified vector with a task-specific mask M_t and a rescaler λ_t . The resulting task-specific weights are $\hat{W}_t = W_{\text{pre}} + \lambda_t \cdot (M_t \odot \tau_{\text{uni}})$.
- **ProDistill** (Xu, Li, and Zhang 2025) formulates model merging as a knowledge distillation problem. It finds element-wise merging coefficients via a progressive, layer-by-layer optimization, minimizing the ℓ_2 distance between the feature embeddings of the merged model and each fine-tuned “teacher” model on a small, unlabeled validation set.
- **AdaMerging** automatically learns a merging coefficient for each layer of each task vector in Task Arithmetic (Ilharco et al. 2023).
- **PCB-Merging** (Du et al. 2024) calculates a score for each parameter through intra-task (self-awareness) and inter-task (cross-awareness) balancing to identify and drop redundant parameters. It then merges the remaining weighted task vectors and can optionally use an evolutionary search algorithm to find optimal per-task merging coefficients.
- **Localize-and-Stitch** (He et al. 2025) identifies tiny sparse regions (γ_t) within each task vector (τ_t) that are essential for performance. These sparse vectors are then stitched back onto the pretrained model using sparse task arithmetic: $\theta_m = \theta_{\text{pre}} + \sum_{t=1}^n (\gamma'_t \odot \tau_t)$, where γ'_t is a processed mask that averages parameters in overlapping regions.

C. Conceptual Comparison of Sparsification Methods in Model Merging

Sparsification has become a basis of modern model merging, serving as the primary mechanism to mitigate task interfer-

| Category | Method | Core Strategy | Sparsification | Data-Free? | Adaptivity Level |
|------------------------|--|--|----------------|------------|---------------------|
| <i>Structure-Aware</i> | TADrop (Ours) | Adaptive pruning based on each tensor’s quantile ratio. | | Yes | Tensor-wise |
| <i>Magnitude-Based</i> | TIES-Merging (Yadav et al. 2023) | Global top-k magnitude pruning. | | Yes | Global |
| | DELLA-Merging (Deep, Bhardwaj, and Poria 2024) | Magnitude-based pruning. | | Yes | Global |
| <i>Structure-Aware</i> | ImPart (Yang et al. 2025a) | SVD-based pruning of singular components. | | Yes | SVD Component |
| | CABS / PCB (Du et al. 2024; Yang et al. 2025b) | Pruning based on inter-task parameter conflict-/competition. | | Yes | Parameter-wise |
| <i>Data-Guided</i> | LEWIS (Chopra, Rambhia, and Adve 2025) | Layer-wise pruning based on activation norms. | | No | Layer-wise |
| | L&S / AdaRank (Lee et al. 2025) | Learns a sparse mask using calibration data. | | No | Parameter/Component |

Table 5: Comparison of sparsification methods in model merging. This table summarizes representative methods based on their core philosophy, data requirements, and level of pruning adaptivity.

ence by pruning redundant or conflicting parameters from task vectors. While the goal is shared, the strategies for identifying *which* parameters to prune vary significantly, revealing different assumptions about the nature of task-specific knowledge. Here, we provide a conceptual comparison of TADrop with contemporary methods. We categorize them by their core sparsification philosophy to highlight the distinct assumptions and mechanisms each approach employs. We summarized the characteristics of each method in Table 5.

Magnitude-Based Sparsification

This foundational category operates on the simple yet effective premise that parameters with larger magnitudes are more critical.

- **TIES-Merging** (Yadav et al. 2023) is a classic example, employing a deterministic *Trim* step that retains only the top- $k\%$ of parameters by magnitude. This global, deterministic pruning serves as a common baseline but treats all parameters homogeneously, ignoring their functional or structural roles.
- **DELLA-Merging** (Deep, Bhardwaj, and Poria 2024) introduces a stochastic variant called *MagPrune*. Instead of a hard threshold, it assigns higher dropout probabilities to parameters with lower magnitudes. This probabilistic approach offers more flexibility than deterministic trimming but still operates on individual parameter magnitudes without considering broader structural context.
- The dataless version of **Localize-and-Stitch** (He et al. 2025) also leverages magnitude-based selection but

pushes it to an extreme, aiming to identify a highly sparse (e.g., top 5%) set of parameters that encapsulates a task’s essence.

These methods share a common characteristic: they operate on the magnitudes of individual parameters and apply a uniform selection criterion across the entire model. This approach does not account for the structural context or varying statistical properties of different parameter groups, a dimension that TADrop is designed to address.

Structure-Aware Data-Free Sparsification

This category includes methods that, like TADrop, are data-free but incorporate more sophisticated, structurally-informed heuristics to guide pruning.

- **SVD-based Methods:** Approaches like **ImPart** (Yang et al. 2025a) shift the focus from the parameter space to the singular value decomposition (SVD) space. ImPart adaptively sparsifies singular vectors based on the magnitude of their corresponding singular values, providing a more granular, importance-aware pruning than simple rank truncation. This acknowledges that importance is not uniform, but does so within the context of SVD components rather than the model’s architectural components.
- **Conflict- and Competition-Aware Methods:** **CABS** (Yang et al. 2025b) introduces a novel structural consideration: orthogonality. Its Conflict-Aware (CA) strategy employs sequential pruning to ensure that the resulting sparse task vectors are non-overlapping, thereby directly minimizing interference. Similarly, **PCB-Merging** (Du

et al. 2024) computes a "Parameter Competition Balancing" score for each parameter, derived from both its intra-task magnitude and inter-task similarity, to guide pruning. These methods explicitly model inter-task relationships to resolve conflicts.

In contrast to methods that analyze singular vectors or model inter-task conflicts, TADrop adopts a different perspective. It assesses the internal statistical distribution of each architectural parameter tensor (e.g., the weight matrix of a query projection). By assigning an adaptive drop rate based on a tensor's quantile ratio, TADrop's adaptivity is guided by the model's inherent architectural structure and the statistical properties of its components.

Data-Guided Sparsification

This category leverages small amounts of data to guide the sparsification process, often achieving high performance at the cost of data dependency and additional computation.

- **Activation-Based Methods:** **LEWIS** (Chopra, Rambia, and Adve 2025) uses a calibration dataset to measure the norm of layer-wise activations. It posits that layers whose activations deviate more significantly from the pretrained model are more critical for the fine-tuned task and should be pruned less aggressively. This introduces adaptivity at the *layer level*, which is coarser than TADrop's tensor-wise approach.
- **Learned Mask Methods: Localize-and-Stitch** (He et al. 2025) and **AdaRank** (Lee et al. 2025) represent the state-of-the-art in data-guided pruning. Localize-and-Stitch learns an extremely sparse binary mask that isolates the most critical parameters for a task by optimizing performance on a small dataset. Similarly, AdaRank learns a binary mask over a task vector's singular components by optimizing an entropy-based objective. These methods can precisely identify critical parameters but require a data-dependent optimization phase.

TADrop distinguishes itself from this category by being entirely data-free. It achieves adaptivity by exploiting the intrinsic statistical properties of the parameters themselves, rather than relying on external data signals like activations or learned masks. This positions TADrop as a lightweight, "plug-and-play" module that offers a more nuanced approach than purely magnitude-based strategies without the overhead and data requirements of guided methods.

D. More Detailed Results

Results for 30 ViT Tasks

This section provides the detailed experimental results for the large-scale merging scenario involving 30 vision tasks, serving as supplementary data for the scalability analysis in the main text. As presented in Table 6, the results highlight a clear performance hierarchy in this challenging, many-task setting. While foundational merging methods like Task Arithmetic, and Ties-Merging suffer from significant performance degradation, TADrop demonstrates its strength when combined with a strong baseline, EMR-Merging, achieving

a top-performing average accuracy of 91.68%. This underscores TADrop's effectiveness in mitigating the escalating task conflict inherent in large-scale merging, therefore, providing empirical support for the robustness and scalability in more challenging, many-task scenarios.

Sensitivity Analysis of Quantile Selection

The performance of TADrop is guided by the Quantile Ratio, which relies on two key hyperparameters, the quantiles a and b . To investigate the method's sensitivity to these parameters, we conducted an analysis on the ViT-B/32 model across eight tasks. We chose quantiles as the basis for our metric due to their inherent robustness to outliers and their effectiveness in capturing the "heavy-tailedness" of parameter distributions, which is central to our hypothesis.

The results, presented in Table 7, show that while the choice of quantiles does influence performance, TADrop exhibits considerable robustness across a range of reasonable values. Performance remains consistently high for various configurations, indicating that the method is not brittle and does not require extensive hyperparameter tuning. Notably, the setting of $a=0.50$ and $b=0.95$ achieved the best average accuracy of 90.72%. Based on these findings, we adopted this optimal and robust configuration for all subsequent experiments.

Intra-Model Sparsity Rates

The main text highlighted the consistent sparsity patterns TADrop assigns across tasks. This section visualizes these patterns in detail for all eight ViT-B/32 tasks. Figure 1 illustrates the adaptive sparsity rates TADrop computes for different ViT parameter tensors across these tasks. Remarkably, despite the diverse data distributions of these tasks (ranging from natural images to satellite imagery and digits), TADrop derives highly similar intra-model sparsification "blueprints." Specifically, consistent patterns emerge: (1) High-Sparsity Components: Certain parameter types, such as `attn_in.b`, consistently receive high drop rates (typically $\geq 80\%$) regardless of the task. (2) Low-Sparsity Components: Conversely, parameters like the weight matrices in Feed-Forward Networks (FFNs) and subsequent LayerNorm are consistently treated more conservatively with lower drop rates.

This high degree of consistency across tasks suggests that different parameter types play distinct and intrinsic roles during the fine-tuning process. We hypothesize that certain parameter types, like attention biases, primarily capture superficial, task-specific information that can be safely pruned to reduce interference, while others, like FFN weight matrices, encode more core, transferable knowledge that should be preserved. This finding provides an explanation for TADrop's success: it is not merely a heuristic but a mechanism that automatically discovers and leverages the distinct functional roles of different components within the Transformer architecture.

| | Pet | Cifar-10 | Cars | MNIST | Kvasir-v2 | Food-101 | Weather | EuroSAT | Vegetables | Cats and Dogs |
|--|-----------------------|------------------------------|--|-------------------------------------|-----------------------------------|------------------------------------|-----------------------|-----------------------|------------------------|-----------------------|
| Individual | 92.23 | 97.88 | 85.06 | 99.22 | 94.31 | 87.94 | 98.21 | 99.11 | 100.00 | 99.03 |
| Weight Averaging | 31.26 | 42.91 | 7.74 | 27.63 | 25.27 | 68.02 | 61.06 | 24.37 | 83.20 | 91.28 |
| RegMean (Jin et al. 2023) | 34.62 | 89.65 | 16.28 | 90.71 | 71.00 | 76.14 | 86.62 | 74.13 | 99.10 | 98.54 |
| Task Arithmetic (Ilharco et al. 2023) | 33.24 | 59.86 | 9.34 | 30.81 | 31.05 | 73.06 | 74.56 | 31.25 | 91.97 | 93.61 |
| Ties-Merging (Yadav et al. 2023) | 12.84 | 42.82 | 5.30 | 23.21 | 21.09 | 73.22 | 72.86 | 10.98 | 92.31 | 91.88 |
| AdaMerging (Yang et al. 2024b) | 48.34 | 87.54 | 0.42 | 81.22 | 22.76 | 75.23 | 89.13 | 44.60 | 97.97 | 96.91 |
| EMR-Merging (Huang et al. 2024) +TADrop | 86.50 90.07 | 96.73 97.91 | 43.50 68.06 | 97.79 98.81 | 84.07 92.43 | 83.22 87.57 | 96.97 97.78 | 97.85 97.22 | 99.96 100.00 | 99.49 99.43 |
| | DTD | Fashion | Dogs | STL-10 | Flowers | LandScape | RESISC45 | EMNIST | Intel-Images | CUB-200-2011 |
| Individual | 71.75 | 93.26 | 89.90 | 99.07 | 98.19 | 94.00 | 98.90 | 94.67 | 94.63 | 91.88 |
| Weight Averaging | 14.63 | 20.46 | 47.80 | 37.74 | 68.97 | 73.14 | 13.56 | 7.73 | 82.40 | 37.66 |
| RegMean (Jin et al. 2023) | 30.53 | 83.42 | 42.89 | 78.94 | 95.26 | 83.64 | 34.66 | 48.67 | 93.60 | 49.78 |
| Task Arithmetic (Ilharco et al. 2023) | 14.73 | 37.11 | 47.65 | 39.66 | 80.68 | 79.59 | 15.50 | 11.05 | 89.03 | 41.86 |
| Ties-Merging (Yadav et al. 2023) | 3.71 | 27.05 | 26.03 | 6.17 | 34.33 | 78.27 | 6.79 | 5.61 | 89.39 | 31.28 |
| AdaMerging (Yang et al. 2024b) | 16.68 | 76.76 | 53.09 | 68.91 | 95.69 | 81.98 | 24.83 | 18.02 | 91.02 | 48.19 |
| EMR-Merging (Huang et al. 2024) +TADrop | 59.62 61.59 | 89.77 91.58 | 86.48 89.67 | 98.23 99.02 | 97.91 97.91 | 94.60 95.00 | 94.80 93.74 | 93.07 93.75 | 95.46 95.43 | 82.86 85.08 |
| | SVHN | Cifar-100 | Beans | SUN397 | Garbage | Animal-10N | Fruits-360 | GTSRB | MangoLeafBD | KenyanFood13 |
| Individual | 96.21 | 89.85 | 96.87 | 87.51 | 98.83 | 92.52 | 100.00 | 95.74 | 100.00 | 82.57 |
| Weight Averaging | 10.88 | 77.98 | 70.98 | 57.42 | 22.89 | 46.00 | 5.38 | 15.00 | 68.58 | 33.55 |
| RegMean (Jin et al. 2023) | 66.13 | 82.59 | 92.58 | 58.58 | 65.31 | 68.74 | 19.79 | 56.96 | 98.10 | 57.11 |
| Task Arithmetic (Ilharco et al. 2023) | 17.41 | 80.20 | 84.62 | 55.88 | 25.23 | 51.14 | 6.15 | 37.01 | 87.02 | 36.32 |
| Ties-Merging (Yadav et al. 2023) | 10.54 | 78.61 | 67.22 | 52.69 | 3.91 | 19.13 | 1.50 | 40.74 | 76.58 | 19.90 |
| AdaMerging (Yang et al. 2024b) | 25.70 | 84.19 | 93.38 | 64.09 | 38.54 | 66.55 | 7.94 | 59.90 | 99.13 | 48.66 |
| EMR-Merging (Huang et al. 2024) +TADrop | 90.56 91.95 | 87.80 90.69 | 95.31 95.31 | 80.92 83.30 | 94.43 94.89 | 88.68 89.60 | 97.40 99.75 | 95.72 96.38 | 99.97 100.00 | 78.52 79.14 |
| <i>Average Performance</i> | | | | | | | | | | |
| Individual | Weight Averaging | RegMean (Jin et al. 2023) | Task Arithmetic (Ilharco et al. 2023) | Ties-Merging (Yadav et al. 2023) | AdaMerging (Yang et al. 2024b) | EMR-Merging (Huang et al. 2024) | TADrop | | | |
| Acc | 93.98 | 42.52 | 68.14 | 48.89 | 37.53 | 60.25 | | 89.61 | | 91.68 |

Table 6: Task-specific and average performance when merging ViT-B/16 models on **30** tasks.

| | SUN397 | Cars | RESISC45 | EuroSAT | SVHN | GTSRB | MNIST | DTD | Avg Acc |
|-------------|--------------|--------------|--------------|--------------|--------------|--------------|--------------|--------------|--------------|
| EMR-MERGING | 75.19 | 72.76 | 93.49 | 99.52 | 96.86 | 98.13 | 99.58 | 74.36 | 88.74 |
| q45/q95 | 78.69 | 78.71 | 95.17 | 99.44 | 97.38 | 98.69 | 99.65 | 77.66 | 90.67 |
| q50/q90 | 78.57 | 78.27 | 95.13 | 99.56 | 97.40 | 98.78 | 99.66 | 78.14 | 90.69 |
| q50/q99 | 78.54 | 78.83 | 94.94 | 99.22 | 97.23 | 98.44 | 99.63 | 77.50 | 90.54 |
| q50/q95 | 78.73 | 78.61 | 95.24 | 99.44 | 97.41 | 98.71 | 99.66 | 77.93 | 90.72 |
| q50/q85 | 78.44 | 77.68 | 95.14 | 99.63 | 97.38 | 98.73 | 99.67 | 77.87 | 90.57 |
| q50/q80 | 78.24 | 77.13 | 95.08 | 99.67 | 97.37 | 98.70 | 99.68 | 77.87 | 90.47 |

Table 7: Performance of different quantile selection on ViT-B/32.

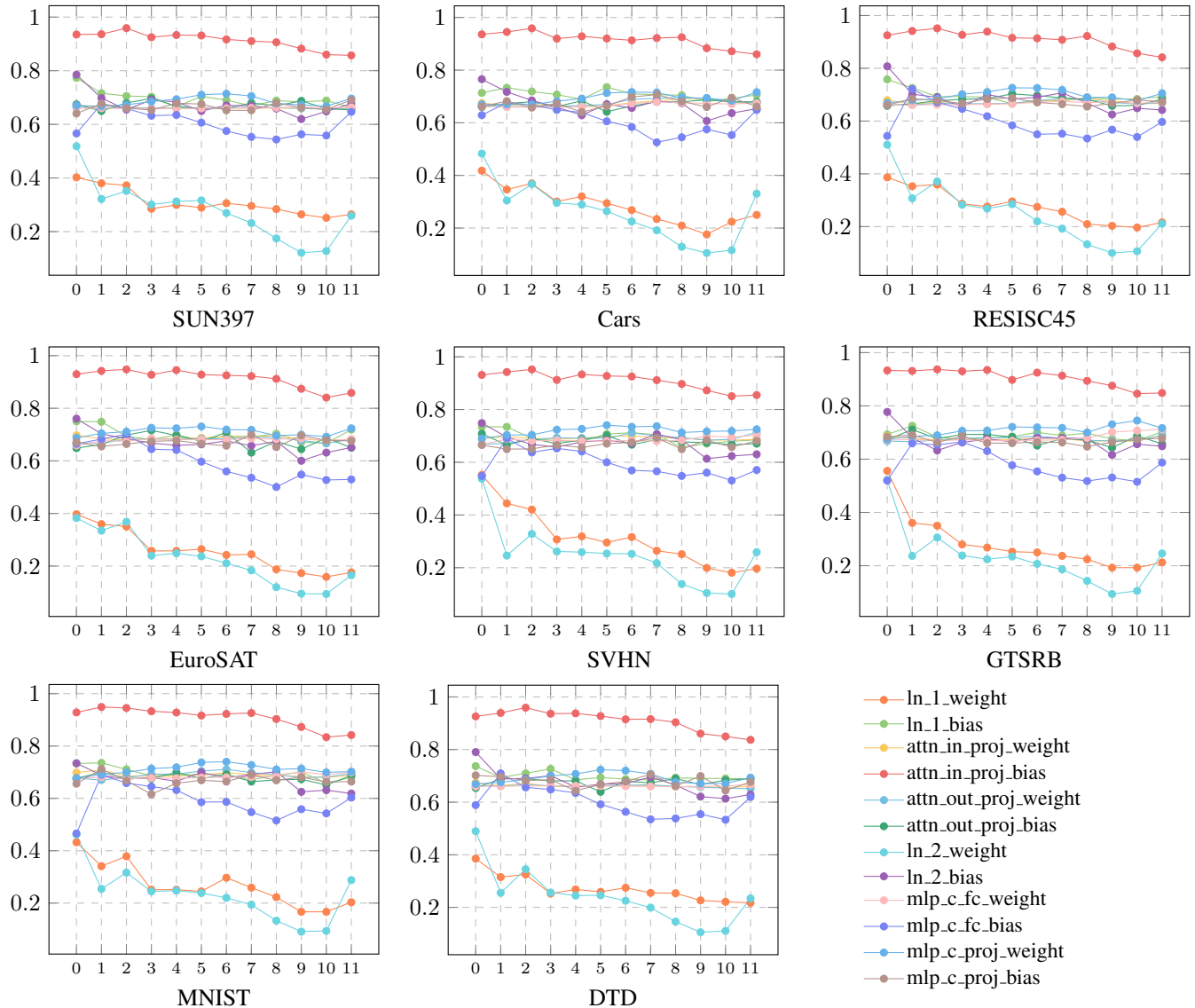


Figure 7: Intra-Model sparsity visualizations for eight ViT-B/32 models.